KSCE Journal of Civil Engineering (2019) 23(5):1999-2008

DOI 10.1007/s12205-019-1092-0

Geotechnical Engineering

pISSN 1226-7988, eISSN 1976-3808
www.springer.com/12205

Behaviors of Wall and Ground due to T-shaped Excavation

Xiaodong Zhao*, Guoqing Zhou, Laijun Qiao***, and Yangguang Chen******

Received August 14, 2017/Revised February 13, 2018/Accepted January 4, 2019/Published Online February 7, 2019

Abstract

Extensive monitoring was performed on a T-shaped site with a length of 280 m, a width of 16 m, and a maximal depth of 20.4 m. The braced excavation was performed under retaining comprised of cast-in-situ bored piles and jet grouting piles. The field data-based wall performance and its influences to ground were assessed by detailed comparisons with that in other excavations. It is showed that the wall deflections, ground movements and bracing forces all exhibited a typical camelback-shaped characteristic along the length direction, and a maximum 100% reduction of which was observed due to the jet grouting. The rebar near sections with varied excavation depths was in a tension state both on the excavation and the retained sides due to the two-dimensional unbalanced force, and the corresponding bracing force was small. The maximum wall deflection δ_{hm} decreased as the partitioning excavation moved horizontally, and it was less than 0.04% of the final horizontal excavation length L_e. The normalized $F_{\sigma max}$ approximately approached to be identical with the normalized F_{bmax}, while most of the occurring depths for $F_{\sigma max}$ were greater than that for F_{bmax}.

Keywords: *T-shaped excavation, large length-width ratio, varied excavation depth, jet grouting, wall and ground behaviors*

1. Introduction

The Coal Preparation Plant (CPP), consisting of bunkers to store disposed coal and preparation facilities, is crucially significant for the achievement of low carbon utilization of high carbon energy by ash removal and desulfurization. The selection of deep foundations is typically used to improve and increase the capacity of the coalbunker, and the successful construction of these foundations requires deep excavation under reliable underpinning.

The focus during excavation is the assessment of deflections of retaining walls, ground movements, and the geo-environmental risks related to seepage and stability. Several approaches have been traditionally utilized to study wall or ground behaviors resulted from excavation, including empirical estimation, laboratory modelling, theoretical assessment and numerical simulation (Qu *et al*., 2000; Osman and Bolton, 2006; Tan and Wang, 2013a, 2013b; Fearnhead *et al.*, 2014; Borges *et al.*, 2014; Tan and Wang, 2015; Liao *et al.*, 2015; Shi *et al.*, 2015; Hsiung *et al.*, 2018). During excavation, a retaining structure may be constructed of soil nailing wall, Cast-in-situ Bored Pile (CBP), Jet Grouting Pile (JGP), or diaphragm wall. Of these temporary underpinning structures, diaphragm walls constructed in slurry-supported, open trenches below existing ground in combination with multi-propped bracing are usually used as the cut-off wall to limit the surrounding ground movement due to the strong structural integrity and the relative high system stiffness of these structures. Extensive field data indicated that this method worked well, especially in congested urban areas characterized by soft and saturated soils. However, for non-urban areas, retaining walls formed by CBPs and JGPs may be an alternative technology to achieve the required stabilization with low costs.

T-shaped excavation strategies protected by walls formed by CBPs and JGPs have been tremendously used for CPP construction in China. However, the empirical or semi-empirical approaches derived from other heteromorphic (such as rectangular, triangular, and cylindrical excavations) and stratified excavations may not yield reliable prediction for T-shaped excavation behavior because excavation behaviors were significantly affected by pit geometries and excavation methods (Tan and Wang, 2013b; Tan and Wang, 2015; Shi *et al.*, 2015). As known, partitioning excavation is applicable for the foundation pits with T-shaped appearance and large length-width ratio. Although extensive studies have addressed stratified excavations, and few have reported partitioning excavations (Qu *et al.*, 2011; Wu *et al.*, 2013).

*Associate Professor, State Key Laboratory for Geomechanics and Deep Underground Engineering, China University of Mining and Technology, Xuzhou, Jiangsu 221116, China (Corresponding Author, E-mail: zxdcumt@126.com)
**Professor, State Key Laboratory for Geomechanics and Deep Underground Engineering, China University of Mining and Technology, Xuzhou, Jiangsu 221116, China (E-mail: gqz@cumt.edu.cn)
***Engineer, Pingdingshan Coal Preparation Design and Research Institute, Beijing Huayu Engineering Co., Ltd., Beijing 100120, China (E-mail: qiaolaijun@bhec.cn)
****Engineer, Dept. of Infrastructure Business, China State Construction Engineering Co., Ltd., Beijing 100044, China (E-mail: yangguang4830@126.com)

Back analysis based on field data is considered to be an effective method to understand structural responses and to evaluate the reliability of initial design and then provide a practical reference for other similar excavations. To perform this analysis, well-documented field data were needed. To date, numerous researchers have conducted monitoring on performances of diaphragm walls (Fearnhead *et al.*, 2014; Tan and Wang, 2015), whereas the retaining effects of JGP walls were not fully understood. Further, the available data was mainly from the numerical observations (Hsieh *et al.*, 2003; Borges *et al.*, 2014; Goh, 2017), and the field data applicable for quantitative analysis in one case with zones treated under different jet grouting thickness was lack.

This paper describes a unique and well–documented case of large-scale foundation pit with T-shaped appearance and large length-width ratio. The foundation pit with a length of 280 m and a width of 16 m, located in Anhui province of China, had a planned area of approximately 5,000 m^2. The walls of this T-shaped excavation was formed by CBPs and JGPs. The partitioning excavation in standard sections with fixed excavation depths and a belt conveyor shaft excavation sections with varied excavation depths were performed under multi-propping. The performance of walls and its influences to grounds were compared with the previously published field data from other sites. Then, the behaviors of wall and ground subjected to partitioning excavation were studied, and the retaining effects of JGP were quantitatively assessed.

2. Background Information

2.1 Ground Conditions

The T-shaped excavation site was proximal to the Huaibei colliery. A coal conveyance trestle and railway were located, respectively, in the west and north of the excavation site, and the existing coalbunker was in the northwestern corner. The soils deposits were mainly from the alluviation of Huaihe River. According to the geological investigation and field exploration as shown in Fig. 1, the soil profile along the excavation depth was stiff clay and dense silt. The soils in this T-shaped excavation were stiffer than that typically distributed in Yangtze River delta (Tan and Wang, 2013a), so the wall comprised of CBPs and JGPs rather than the diaphragm wall was adopted. And the field observations in the following sections validated that the alternative method was effective.

The groundwater level was apparently shallow and there were water resources at the CPP construction site. The depth of the groundwater ranged from 0.8 to 2.1 m and was supplied mainly by precipitation as well as the infiltration of ground surface water. The fluctuation amplitude of the groundwater level was approximately 2.0 m due to rainfall and evaporation. The elevation of groundwater level in the T-shaped excavation site was about −5.0 m.

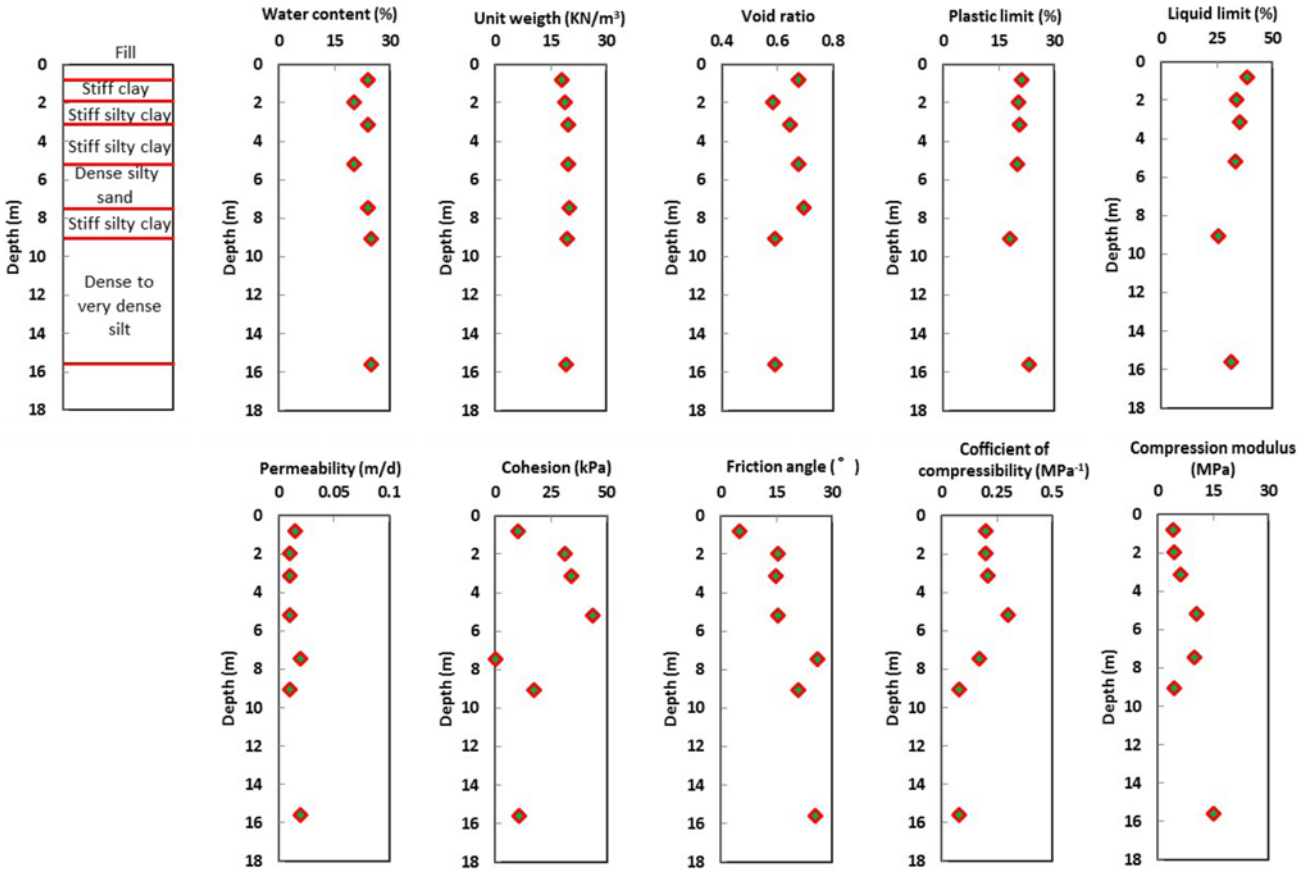

Fig. 1. Physical Properties and Mechanical Parameter Profiles at the Excavation Site

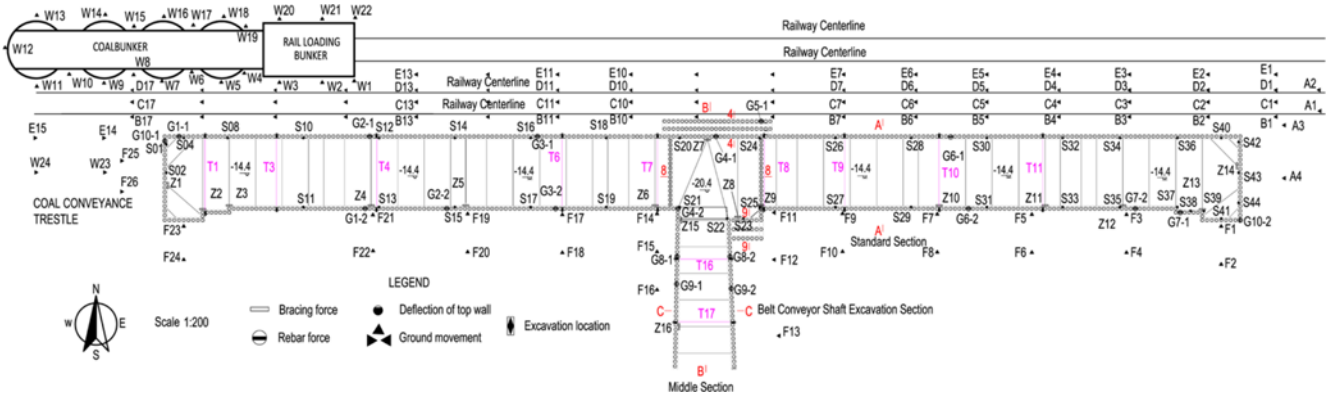

Fig. 2. Excavation Site and the Monitoring Points

2.2 Descriptions of Retaining Walls

The excavation site had a length of 280 m and a width of 16 m, and presented a T-shaped appearance as shown in Fig. 2. The CBP had a diameter of 0.80 m and a concrete grade of C30, and formed the cut-off walls together with the neighboring high-pressure JGP with a diameter of 0.7 m. The overlapping thickness of the JGP was 0.10 m, and the compressive strength was greater than 5.0 MPa.

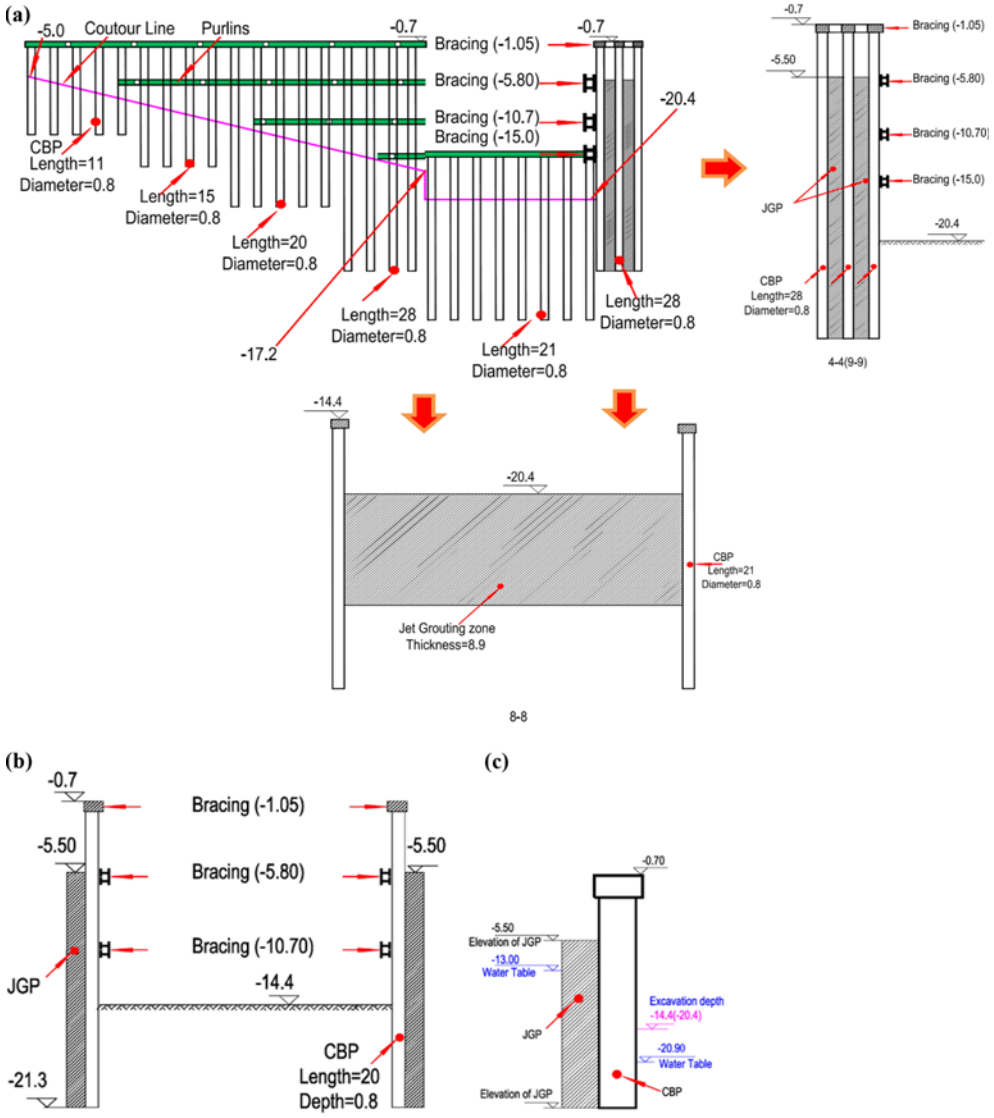

Fig. 3. Retaining Walls: (a) Details of Middle Section: B-B, (b) Walls under Standard Section: A-A, (c) Water Table (unit: m)

The wall of CBP and the wall of JGP were arranged alternately in middle section B-B in the width direction of the foundation pit as shown in Fig. 3(a). And there were 5 lengths (11 m, 15 m, 20 m, 28 m and 21 m) along the south-north direction. Whereas the length of CBP in standard sections was 20 m, and a single wall of JGP was adopted as shown in Fig. 3(b). In Fig. 2, A-A section was a typical standard section, and C-C section was in the zones for belt conveyor shaft excavation.

Additionally, the lateral earth pressure was transferred by the compressive struts. The steel pipes were used as the struts, and were installed between the retaining walls at two sides, to limit the deformations of the retaining walls. The thickness and the outer diameter of steel pipes were 0.016 m and 0.609 m respectively. These steel pipes were divided into three levels under the standard sections, and the elevations were −1.05 m, −5.8 m and −10.7 m, respectively. The bracing under an elevation of −15.0 m was specially added in the middle section B-B due to the relatively great excavation depth.

Further, three elevations of bracing near section C-C shown in Fig. 2 gradually reduced to two elevations, and finally to one elevation as shown in Fig. 3(a). In order to reduce the instantaneous displacement of walls at the initial stages, preloading of 200 KN was applied to bracing under a depth of −1.05 m via the hydraulic jack, and 500 KN was used for the depths greater than −1.05 m.

The control of the underground water level was achieved comprehensively by jet grouting and tube well dewatering. The JGP was designed in two rows along the east-west direction forming a tier wall under standard sections as shown in Fig. 3(b), and three rows forming two tiers walls at the corners in section 4-4 and section 9-9, as shown in right part of Fig. 3(a). The thickness of jet grouted zone beneath excavation depth of 20.4 m was 8.9 m as shown in bottom part of Fig. 3(a). Additionally, there were 69 dewatering wells with a diameter of 0.5 m and a depth of 25 m that were arranged around the excavation site at an interval of 15 m. As shown in Fig. 3(c), the anticipated groundwater level was maintained at an elevation of −13.0 m close to the excavation site, but there was a 0.5 m deviation for the elevation between the expected groundwater level and the corresponding excavation depth in the construction site.

The final elevation depth of the standard sections along the east-west direction as shown in Fig. 3(b) was 14.4 m. The final excavation depth varied from 5.0 to 17.2 m, showing gradual linear change in the middle section B-B shown in left part of Fig. 3(a), and the maximum excavation depth neighboring to depth of 17.2 m was 20.4 m. The correspondent CBP length was therefore ranging from 11 m to 28 m. Further, the elevations of the JGP and CBP were −5.5 m and −0.7 m both in middle section B-B and standard sections.

Shortening the excavation period is recognized to contribute to ground control and reduce the potential hazards of ground movements on the environment and adjacent infrastructures or facilities. The duration of this project was 218 days, and the duration of the excavation course was about 63 days as indicated in Tables 1 and 2, and that was divided into 6 stages based on the in-situ feedback information. The partitioning excavation was initiated from the east and west side, and then was performed in the middle section after finishing the standard sections in the east-west direction. The excavation progress was accelerated in the middle section due to the potential threat from the maximal excavation depth. The connection of the cap beam with the piles can increase the wall stiffness and decrease the lateral deflection and ground movements. Therefore, the excavation was continued after the cap beam was casted. The bottom-up method was adopted in the excavation, and the basal slab was constructed

Table 2. Details for Stage 2 and Stage 5

Stage	Date	Construction activity
2	2011.11.26–2011.11.29	Excavate to level 1 (−1.57 m)
		Cast prop (−1.07 m)
	2011.11.30–2011.12.03	Excavate to level 2 (−6.3 m)
		Cast prop (−5.8 m)
	2011.12.04–2011.12.08	Excavate to level 3 (−14.4 m)
		Cast prop (−10.7 m)
	2011.12.09–2011.12.10	Cast slab
5	2011.12.29	Excavate to level 1 (−1.57 m)
		Cast prop (−1.07 m)
	2011.12.30	Excavate to level 2 (−6.3 m)
		Cast prop (−5.8 m)
	2011.12.31	Excavate to level 3 (−14.4 m)
		Cast prop (−10.7 m)
	2012.01.01	Excavate to level 3 (−15.5 m) Cast prop (−15.0 m)

Table 1. Excavation Course

Stage	Date (year/month/day)	Duration (days)	Excavation location (m) (from the east side)	Excavation location (m) (from the west side)
1	2011.11.09–2011.11.25	17	T11(51.2)	T1(10.05)
2	2011.11.26–2011.12.10	15	T10(78.6)	T3(29)
3	2011.12.11–2011.12.20	10	T9(103.6)	T4(55.3)
4	2011.12.21–2011.12.28	8	T8(124.8)	T6(104.4)
5	2011.12.29–2012.01.01	4	between T8 and T7	T7(129.5)
6	2012.01.02–2012.01.10	9	T16 (28.6 m from the south side)	
7	2012.01.11–2012.05.13	124	Casting of base slab, subsurface construction of main structures of coalbunker	
8	2012.05.14–2012.06.13	31	Construction of facilities above the ground	

Fig. 4. Pictures of In-situ Monitoring: (a) Wall Deflection, (b) Rebar Force, (c) Bracing Force

when the excavation depth reached the final level. The bracing strut was removed when the permanent concrete structures were constructed.

2.3 Monitoring Strategy and Instrumentation

There were several components of monitoring the excavation: 1) The lateral movement of the retaining walls comprised of CBPs and high-pressure JGPs was measured by 46 deflection monitoring points (S1-S46) as shown in Fig. 4(a). 2) Ground settlements located at 30 m around the excavation site were monitored by surveys of 60 deflection monitoring points (F1-F26, C1-C17, E1-E15, and A3-A4) and there were 60 movement monitoring points of survey nails that surrounded the adjacent railway (B1-B17, D1-D17, A1-A2) and infrastructures (existing coalbunker and trestle for coal conveyance) (W1-W24). 3) The strut forces (Z1-Z16) under 16 sections measured by 48 vibrating wire strain gauges that was distributed at each level of bracing and the rebar forces (G1-G10) under 10 sections were measured by vibrating wire strain gauges distributed at an interval of 2.0 m as shown in Figs. 4(b) and 4(c).

3. Field Measurement

3.1 Wall Deflection

Typically, the wall develops typical deep-seated lateral movements during the process of excavation, particularly as it reaches the deep layers, with the maximum deflection close to the excavation base (Tan and Wei, 2012; Tan and Wang, 2013a; Shi *et al.*, 2015). It was concluded from the data shown in Fig. 5 that the maximum wall deflection δ_{hm} after the final excavation was about 0.54 times more than the top wall deflection δ_h based on the reported data from Li *et al.* (2012) and Tan and Wang (2013b), where S1-S44 were the monitoring points shown in Fig. 2. The inclinometers were not used in this field measurement, so the maximum wall deflection δ_{hm} in the T-shaped excavation was calculated using the following equation:

$$\delta_{hm} = \delta_h/0.54 \quad (1)$$

To better understand the potential effects of the geometric conditions on wall deflections, field data from basement excavations and metro station excavations in Shanghai were compared with the cylindrical shafts (Tan and Wang, 2013a). The measured δ_{hm} was around δ_{hm} = 0.1% H to δ_{hm} = 1.0% H for the basement excavation and δ_{hm} = 0.02% H to δ_{hm} = 0.5% H for the metro excavations, where H was the excavation depth. From Fig. 5, the observed δ_{hm} was around δ_{hm}/H_e = 0.02% to δ_{hm}/H_e = 0.43%, a range that was in agreement with the reported range from the metro excavations (Wang *et al.*, 2005; Tan and Wei, 2012), but smaller than that from the building basement excavation (Xu, 2007) and larger than that from the cylindrical excavation (Tan and Wang, 2013a), where H_e was the final excavation depth. Furthermore, the location of δ_{hm}/H_e = 0.43% was found to be at the east side of the T-shaped excavation site because the excavation was initiated from the east side, and this process likely dominated the subsequent wall deflections. Three zones, the zone at the east or west side along the width direction, the

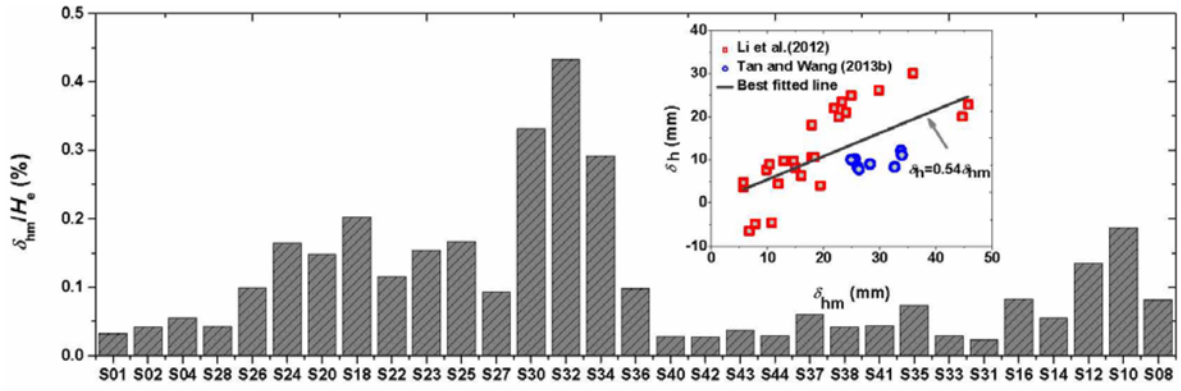

Fig. 5. δ_{hm}/H_e at Different Monitoring Points

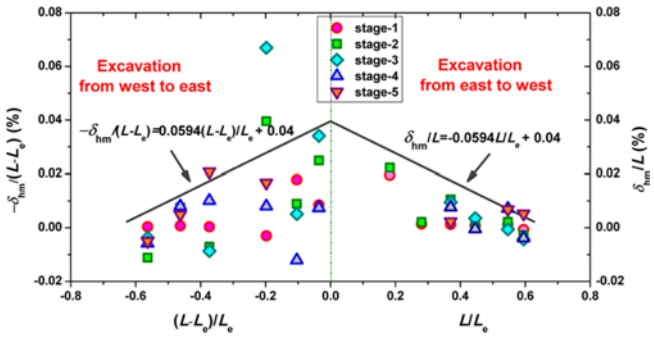

Fig. 6. L/L_e versus δ_{hm}/L and $(L-L_e)/L_e$ versus $-\delta_{hm}/(L-L_e)$

zone around the middle section, and the zone in the length direction of the excavation site, are seen from the data presented in Fig. 5. Obviously, the maximum deflection δ_{hm} for retaining walls located at the east and west side of the excavation site and in zones around the middle sections were smaller than that of the third zone due to the geometry and the local strengthening via jet grouting.

Compared with the duration for horizontal excavation, the duration for vertical excavation to the slab under each stage was much shorter. It was therefore necessary to explore the relationship between the horizontal excavation distance L between the monitoring point and the east side and the maximum wall deflection δ_{hm}. The final horizontal excavation distance was L_e = 280 m, the distance between the monitoring point and the west side was therefore $L–L_e$. As shown in Fig. 6, Table 1 and Fig. 2, all the measured δ_{hm}/L or $-\delta_{hm}/(L–L_e)$ under each stage decreased as the excavation moved forwards with the exception of three points on the west side. The notable decreasing of δ_{hm}/L was observed at east side under the initial excavation stages, corresponded to $L/L_e \le 0.2$, and started to stabilize when $L/L_e \ge 0.2$. The maximum deflection on the west side was expected to be greater than that on the east side because of the effects of the existing coalbunker and railway. Nevertheless, the overall excavation speed in the western zone was greater than that in the eastern zone, and there was inadequate time for wall deflection development. Accordingly, the excavation-induced wall defections approached nearly identical with that in the east side, Further, δ_{hm}/L and $-\delta_{hm}/(L–L_e)$ in Fig. 6 showed a symmetric characteristic, and all δ_{hm}/L and $-\delta_{hm}/(L–L_e)$ data except $-\delta_{hm}/(L–L_e)$ = 0.20 under stage 2 and stage 3 in west side fell into a narrow range formed by the following:

$$\delta_{hm}/L = -00594L/L_e + 0.04,\ -\delta_{hm}/(L–L_e) = 0.0594(L–L_e)/L_e + 0.04, \text{ and } \delta_{hm}/L = -0.01 \quad (2)$$

3.2 Rebar Force

To investigate the bending stresses in the wall panels composed of CBPs and JGPs during excavation, the measured vertical stresses of G3-1 and G9-1 at $H = H_e$ were plotted against depth in Fig. 7, where symbols of "+" and "–" represent the tension and compression, respectively, G9-1 was near C-C section, and G3-1

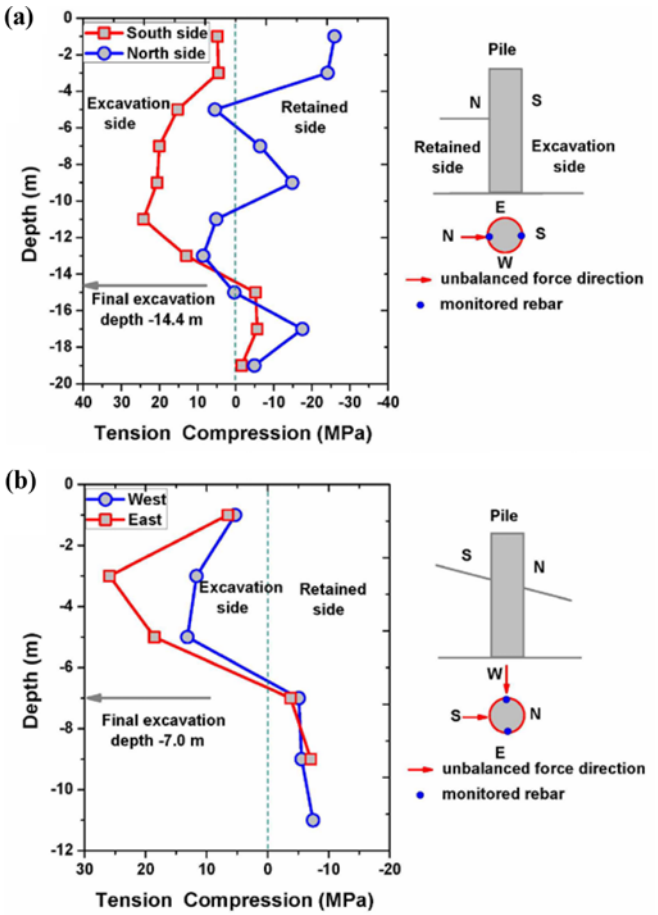

Fig. 7. Rebar Force under: (a) Standard Section, (b) Section Near C-C

was in a typical standard section. As expected, the wall panels in standard excavation sections were in a tensile state on the excavation side and most monitoring points were in a compressive state on the retained side due to the bulging-type inward wall deflections (Tan and Wang, 2015). The reason can be attributed to the performing of bracing under first and second elevation. It can also be seen from the data in Fig. 7(a) that the rebar force presented an increasing, and then a decreasing trend as the embedded depth increased. In addition, the inflection point was located at a depth of approximate 10 m, in the lower half of the final excavation depth. It implies that the maximal deflection was located at the lower-middle parts of the excavation depth. This observation agreed well with the previous studies (Qu *et al.*, 2000; Tan and Wang, 2015). However, in Fig. 7(b), the rebar force in piles under the middle section B-B with varied excavation depths shown in Fig. 3(a) was different from that under the standard sections. Specifically, the location of maximum rebar force on the excavation side occurred under a depth of 3 m, which was located at the upper-middle portion of the excavation depth, and the rebar force was in a tension state on the retained side. This discrepancy might be related to the two-dimensional unbalanced force induced from varied excavation depth. The tension stress from the bending deflection in the north-south

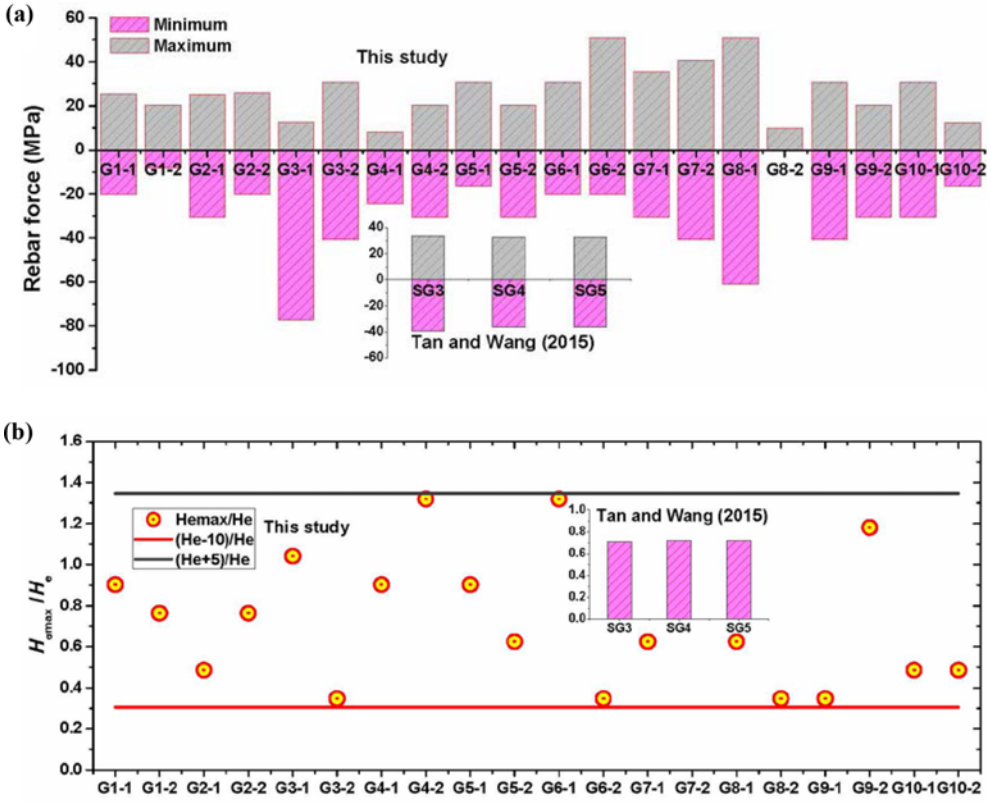

Fig. 8. Maximum and Minimum: (a) Rebar Force, (b) Their Occurrence Depth

direction neutralized the compression stress from the bending deflection occurring in the east-west direction.

Figure 8(a) depicts the measured maximum and minimum rebar force, where G1-1-G10-2 was the monitoring points as shown in Fig. 2, 1 to 10 behind "G" stands for different monitored sections, 1 and 2 behind "–" represent locations at the north and south sides of the excavation site. The minimum and maximum rebar force was found in pile G8-1 and G3-1 with a value of −77.4 MPa and 50.9 MPa respectively, and the averaged rebar force was about −31.1 MPa and 26.6 MPa respectively. To assess the performance of walls formed by CBPs and JGPs, the field data from a cylindrical excavation in Shanghai (SG3, SG4, and SG5) (Tan and Wang, 2015) was analyzed. The maximal and minimal averaged stress of rebar in the circular diaphragm wall was 32.7 MPa and −37.3 MPa respectively, were greater than that occurred in this T-shaped excavation. The noticeable wall deflections observed in Fig. 5 might be from the translational motion of piles, and bending-induced deflections contributed little to the observed deflections due to the multi-propping and decreased constraining effects from a weak cap beam integrity. Consequently, the measured rebar force from bending exhibited a reducing trend. Additionally, it is seen from Fig. 8(b) that the ratio between depth for maximal force $H_{\sigma max}$ and the final excavation depth H_e was about from $H_{\sigma max}/H_e = 0.35$ to $H_{\sigma max}/H_e = 1.32$. The measured $H_{\sigma max}/H_e$ was within the lower limit $(H_e - 10)/H_e$ and the upper limit $(H_e + 5)/H_e$. The averaged $H_{\sigma max}/H_e = 0.73$ in the T-shaped excavation was almost identical to $H_{\sigma max}/H_e = 0.72$ for the circular excavation (Tan and Wang, 2015). Despite some outlying data, it is encouraging to see that the rebar force in the walls formed by CBPs and JGPs was apparent smaller than that in the circular walls. Considering the low cost and high efficacy of this approach, the retaining structures comprised of CBPs and JGPs might be an acceptable strategy in non-urban areas.

3.3 Bracing Force

From Fig. 9, the maximum bracing force occurred at a depth of 10.5 m, which matched well with the location of the inflection point observed in Fig. 7(a), where Z1-Z15 was the monitoring points shown in Fig. 2. However, the bracing force under sections with varied depth near section C-C was smaller than the force in other sections due to the apparent shallow H_e and the two-dimensional non-balanced forces. As illustrated in Fig. 9

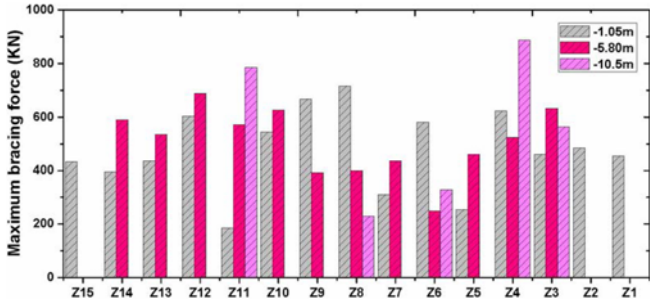

Fig. 9. Maximum Bracing Force

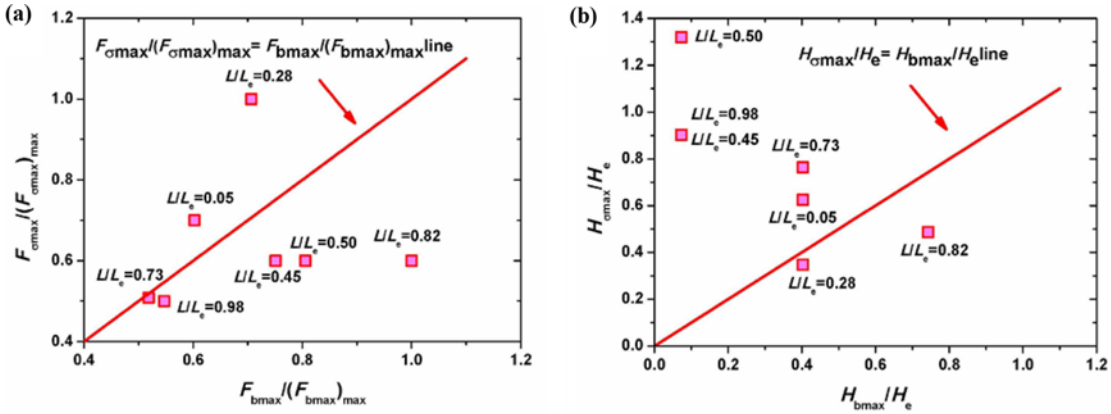

Fig. 10. Comparison between the Rebar Force and Bracing Force: (a) Normalized Force, (b) Occurrence Depth

and Fig. 2, the bracing force under $H = H_e$ exhibited typical camelback-shaped characteristics along the length direction of the T-shaped excavation site, and the maximum of 887 KN was found at Z11. This phenomenon was directly associated with the asymmetric ground movements and wall deflections. In other words, the larger settlement of ground behind the retaining walls led to a greater wall deflection and thus producing a greater bracing force.

To investigate the relationship between maximum rebar force $F_{\sigma max}$ and maximum bracing force F_{bmax}, the normalized $F_{\sigma max}$ and F_{bmax} under different L/L_e are shown in Fig. 10(a), where $F_{\sigma max}$ and F_{bmax} were the maximum value for each monitoring point, and they were separately normalized by the maximum value among them. The corresponding locations H_{bmax}/H_e for F_{bmax} and $F_{\sigma max}/H_e$ for $F_{\sigma max}$ are shown in Fig. 10(b). The data in Fig. 10 were collected from Figs. 8 and 9. As shown in Fig. 10, the normalized $F_{\sigma max}$ approximately approached to be identical with the normalized F_{bmax} despite some fluctuations under a large level of $F_{\sigma max}$ and F_{bmax}. However, most of the occurrence depths $H_{\sigma max}/H_e$ for $F_{\sigma max}$ were greater than H_{bmax}/H_e for F_{bmax}. This is induced by the coupling between CBPs and steel pipes in retaining system.

3.4 Ground Settlements

Figure 11 plots the relationship between the maximum ground settlement δ_{vm}, and the distance, d, behind the retaining walls under $H = H_e$, in which δ_{vm} and d were normalized by H_e, B1-D17 were the monitoring points shown in Fig. 2. As expected, the ground settlements in this study showed a typical concave profile, i.e., the maximum δ_{vm} did not occur right behind the wall but in a zone near $0.3H_e$ outside the wall because the interaction between the retaining walls and the soil deposits restricted the neighboring ground subsidence. The maximum $\delta_{vm}/H_e = 0.25\%$ was a little larger than the $\delta_{vm}/H_e = 0.20\%$ proposed by Hashash *et al.* (2008), but smaller than $\delta_{vm}/H_e = 0.97\%$ reported by Peck (1969), and $\delta_{vm}/H_e = 0.40\%$ computed by Tan and Wang (2013a) based on the peripheral rectangular pit excavation in Shanghai soft clay. Although the characteristics of the $\delta_{vm}/H_e - d/H_e$ data was similar with the trend of the data from Tan and Wang (2013a), the measured δ_{vm}/H_e was smaller than δ_{vm}/H_e in the data presented by Tan and Wang (2013a) when $d \le 0.33H_e$ except a value of $\delta_{vm}/H_e = 0.30\%$, and the observed δ_{vm}/H_e was larger than that value for the data from Tan and Wang (2013a) when $d \ge 0.33H_e$. A new prediction curve was established when an increment of 0.1 was considered on the basis of the prediction curve proposed by Xu (2007). Then, all the measured δ_{vm}/H_e were above this new prediction curve. Additionally, the horizontal ground movements δ_{ghm} in most monitoring points were smaller than the vertical movement δ_{vm}, because δ_{ghm}/δ_{vm} was approximately from $\delta_{ghm}/\delta_{vm} = 0.2$ to $\delta_{ghm}/\delta_{vm} = 1.6$ with an averaged $\delta_{ghm}/\delta_{vm} = 0.6$ as shown in Fig. 11(b).

As described above, the integrity of the retaining wall connected with the cap beam was easily interrupted by the multi-step

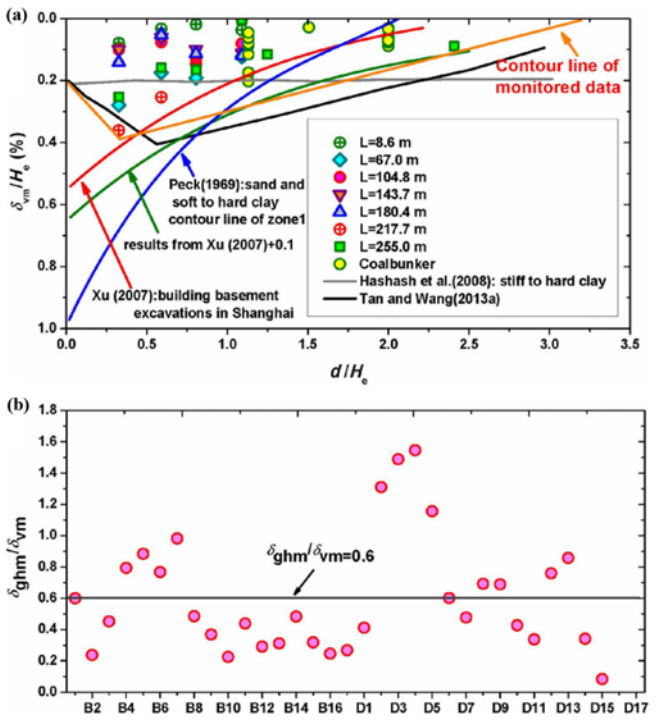

Fig. 11. Ground Settlement Profiles versus Those predicted by Empirical Methods: (a) δ_{vm}/H_e versus d/H_e, (b) δ_{ghm}/δ_{vm}

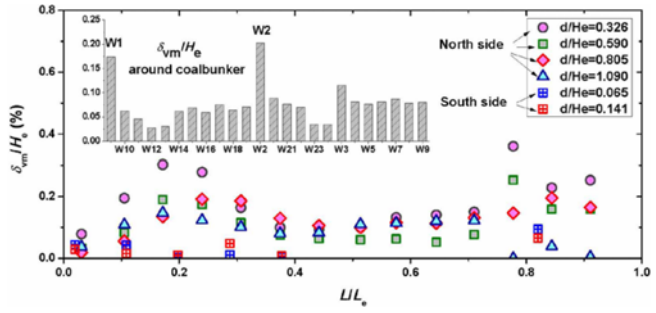

Fig. 12. Relationship between δ_{vm}/H_e and L/L_e

excavation and multi-step construction, thus resulting in a marked reduction of system stiffness. This reduction of system stiffness together with the locally distributed heavy haul railway and coalbunker together promoted ground movement and its non-uniformity. Additionally, corner effects resulted from the irregular geometry and the large ratio between length and width enhanced the asymmetric nature of this moving behaviors. In order to better illustrate the distribution of normalized ground settlement in the east-west direction of the excavation site, Fig. 12 presents the relationship between δ_{vm}/H_e and L/L_e. The measured data near the existing coalbunker is also presented in Fig. 12 for comparison, where W1-W24 is the measuring points shown in Fig. 2. As shown in Fig. 12, the δ_{vm}/H_e curve showed a typical camelback-shaped characteristic, and the minimal δ_{vm}/H_e = 0.1% was in L/H_e = 0.5 with a maximum excavation depth of 20.4 m, and the maximal $\delta_{vm}/H_e \geq 0.2\%$ was about in the range of L/H_e = 0.2 and L/H_e = 0.8. The value of $\delta_{vm}/H_e \leq 0.2\%$ at the south side of coalbunker was larger than $\delta_{vm}/H_e \leq 0.09\%$ observed at the north side of the coalbunker due to the decreasing of influencing range. This value was significantly smaller than those observed at the settlements near the railways L/H_e = 0.2 and L/H_e = 0.8. Additionally, δ_{vm}/H_e = 0.03% that was observed at the west side of coalbunker was much lower than δ_{vm}/H_e = 0.08% observed at the east side of coalbunker due to the effects of loading bunker and corner effects. Particularly, the settlement that occurred at W1 or W2, monitoring points located closer to the cylindrical coalbunker, was more significantly affected by rail moving, and was therefore 2 to 6 times greater than that around the coalbunker.

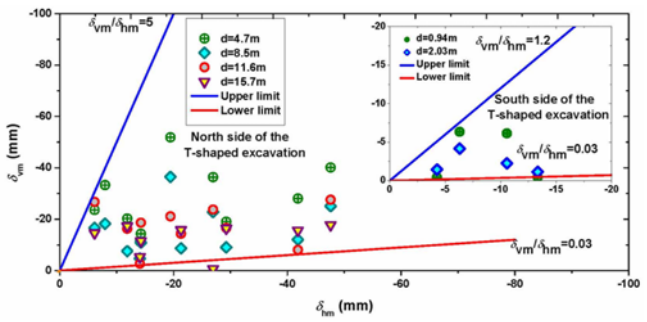

Fig. 13. Relationship between δ_{vm} and δ_{hm}

Figure 13 plots the relationship between the maximum wall deflections, δ_{hm}, and the corresponding maximum ground settlements, δ_{vm}, behind the retaining walls, where the blue and red lines were the upper and lower limits of the measured data respectively. The observed δ_{vm} at the north side in this T-shaped excavation was between δ_{vm} = 0.03 δ_{hm} and δ_{vm} = 5.0 δ_{hm}, it was between δ_{vm} = 0.3 δ_{hm} and δ_{vm} = 1.5 δ_{hm} for the cylindrical excavation (Tan and Wang, 2013a), and between δ_{vm} = 0.3 δ_{hm} and δ_{vm} = 2.0 δ_{hm} for the basement excavation (Xu, 2007). Obviously, the observed δ_{vm}/δ_{hm} in this study exhibited a wider range than that reported for the cylindrical and basement excavations. However, the railway and the trail movement exerted a strong influences on ground movements. As a result, the measured δ_{vm} ranging from δ_{vm} = 0.33 δ_{hm} to δ_{vm} = 1.2 δ_{hm} at the south side was smaller than that at the north side.

The reported cylindrical excavation and basement excavation all occurred at Yangtze River delta alluvial plain. Although the soft soil deposits usually existed under apparent shallow excavation depths, the stiff clays were found in apparent great excavation depth. And the soil deposits in this T-shaped excavation was mainly stiff clays and dense silt. So, the comparisons between cylindrical and T-shaped excavation was reasonable and the findings were reliable. And the recognitions to the behaviors of walls and grounds contribute to better understand and assess the field performance of retaining structures. The energy saving and environmental protection promote the emergence of CPPs, thus producing numerous T-shaped and excavations with great length-width ratio. The above mentioned field monitoring and the back analysis provide an evaluation criterion for retaining design and a correct orientation for the subsequent optimization. Particularly, the JGP initially adopted as the waterproof barrier should be re-considered in the soil retaining.

4. Conclusions

A multi-braced partitioning excavation with different final depths and varied depth was used in an instrumented foundation pit with T-shaped appearance and large length-width ratio. The field data were well documented and detailedly compared with that derived from other excavations .Then, the behaviors of wall and ground were studied and the influences of jet grouting were quantitatively interpreted. The following major findings and conclusions were reached:

1. The wall deflection δ_{hm}/L or $-\delta_{hm}/(L-L_e)$ decreased as the excavation moved horizontally, and a symmetric characteristic between δ_{hm}/L at east and $-\delta_{hm}/(L-L_e)$ at west parts of the T-shaped excavation was observed. Further, most δ_{hm}/L and $-\delta_{hm}/(L-L_e)$ data fell into a zone limited by the following:

$$-\delta_{hm}/(L-L_e) = 0.0594L/(L-L_e) + 0.04,\ \delta_{hm}/L = -0.0594L/L_e + 0.04, \text{ and } \delta_{hm}/L = -0.01 \quad (3)$$

2. The rebar near the sections with varied excavation depth was in a tension state both on the excavation side and the

retained side due to the two-dimensional unbalanced force, and the corresponding bracing force was small. The normalized $F_{\sigma max}$ approximately approached identical with the normalized F_{bmax}, but most of the occurring depths for $F_{\sigma max}$ were greater than F_{bmax}.

3. The ground settlement δ_{vm}/H_e, similar with wall deflection and bracing force, showed typical camelback-shaped characteristics along the length direction, and a maximum 100 % reduction of which due to jet grouting was observed. Further, the level and the range of δ_{vm}/H_e at north side of the excavation site was greater than that at the south side due to the coalbunker and railway.
4. The maximal or minimal averaged $F_{\sigma max}$ and δ_{hm}/H_e in T-shaped excavation approximately approached that occurred in excavations retained by diaphragm walls despite a wider range of δ_{vm}/H_e. Therefore, a wall comprised of CBPs and JGPs has a good retaining performance, and is applicable for heteromorphic excavations in non-urban areas.

Acknowledgements

The authors are grateful to the Fundamental Research Funds for the Central Universities (Grant No. 2015XKQY17), for financial support. The authors also appreciate the assistance contributed by other group members for field monitoring.

References

Borges, J. L. and Guerra, G. T. (2014). "Cylindrical excavations in clayey soils retained by jet grout walls: Numerical analysis and parametric study considering the influence of consolidation." *Computers and Geotechnics*, Vol. 55, No. 1, pp. 42-56, DOI: 10.1016/j.compgeo.2013.07.008.

Fearnhead, N., Standing, J. R., Maniscalco, K., and Wan, M. S. (2014). "Deep excavations: Monitoring mechanisms of ground displacement." *Geotechnical Engineering*, Vol. 67, No. GE2, pp. 117-129, DOI: 10.1680/geng.13.00047.

Goh, A. T. C. (2017). "Deterministic and reliability assessment of basal heave stability for braced excavations with jet grout base slab." *Engineering Geology*, Vol. 218, pp. 63-69, DOI: 10.1016/j.enggeo.2016.12.017.

Hashash, Y. M. A., Osouli, A., and Marulanda, C. (2008). "Central artery/tunnel project excavation induced ground deformations." *Journal of Geotechnical and Geoenvironmental Engineering*, Vol. 134, No. 9, pp. 1399-1406, DOI: 10.1061/(ASCE)1090-0241(2008)134:9(1399).

Hsieh, H. S., Wang, C. C., and Ou, C. Y. (2003). "Use of jet grouting to limit diaphragm wall displacement of a deep excavation." *Journal of Geotechnical and Geoenvironmental Engineering*, Vol. 129, No. 2, pp. 146-157, DOI: 10.1061/(ASCE)1090-0241(2003)129:2(146).

Hsiung, B. C. B., Yang, K. H., Aila, W., and Ge, L. (2018). "Evaluation of the wall deflections of a deep excavation in Central Jakarta using three-dimensional modeling." *Tunneling and Underground Space Technology*, Vol. 72, pp. 84-96. DOI: 10.1016/j.tust.2017.11.013.

Li, S., Zhang, D. L., Fang, Q., and Li, Z. J. (2012). "Research on characteristics of retaining wall deformation due to deep excavation in Beijing." *Chinese Journal of Rock Mechanics and Engineering*, Vol. 31, No. 11, pp. 2344-2353 (In Chinese), DOI: 10.3969/j.issn.1000-6915.2012.11.024.

Liao, S. M., Wei, S. F., Tan, Y., and Liu, J. X. (2015). "Field performance of large-scale deep excavations in Suzhou." *Chinese Journal of Geotechnical Engineering*, Vol. 37, No. 3, pp. 459-469 (In Chinese) DOI: 10.11779/CJGE201503009.

Osman, A. S. and Bolton, M. D. (2006). "Design of braced excavations to limit ground movements." *Geotechnical Engineering*, Vol. 159, No. GE3, pp. 167-175, DOI: 10.1680/geng.2006.159.3.167.

Ou, C. Y., Hsieh, P. G., and Lin, Y. L. (2011). "Performance of excavations with cross walls." *Journal of Geotechnical and Geoenvironmental Engineering*, Vol. 137, No. 1, pp. 94-104.

Peck, R. B. (1969). "Deep excavation and tunneling in soft ground. State-of the-art-report." *Proc., 7th Int. Conf. of Soil Mechanics and Foundation Engineering*, International Society of Soil Mechanics and Geotechnical Engineering (ISSMGE), Mexico City, Mexico, pp. 225-281.

Qu, C. Y., Liao, J. T., and Cheng, W. L. (2000). "Building response and ground movements induced by a deep excavation." *Geotechnique*, Vol. 50, No. 3, pp. 209-220, DOI: 10.1680/geot.2000.50.3.209.

Shi, J. W., Liu, G. B., Huang, P., and Ng, C. W. W. (2015). "Interaction between a large-scale triangular excavation and adjacent structures in Shanghai soft clay." *Tunneling and Underground Space Technology*, Vol. 50, pp. 282-295, DOI: 10.1016/j.tust.2015.07.013.

Tan, Y. and Wang, D. L. (2013a). "Characteristics of a large-scale deep foundation pit excavated by the central-island technique in Shanghai soft clay. I: Bottom-up construction of the central cylindrical shaft." *Journal of Geotechnical Geoenvironmental Engineering*, Vol. 139, No. 11, pp. 1894-1910, DOI: 10.1061/(ASCE)GT.1943-5606.0000928

Tan, Y. and Wang, D. L. (2013b). "Characteristics of a large-scale deep foundation pit excavated by the central-island technique in Shanghai soft clay. II: Top-down construction of the peripheral rectangular pit." *Journal of Geotechnical Geoenvironmental Engineering*, Vol. 139, No. 11, pp. 1894-1910, DOI: 10.1061/(ASCE)GT.1943-5606.0000929.

Tan, Y. and Wang, D. L. (2015). "Structural behaviors of large underground earth retaining systems in Shanghai. I: Un-propped circular diaphragm wall." *Journal of Performance of Constructed Facilities*, Vol. 29, No. 2, pp. 04014058-1-14, DOI: 10.1061/(ASCE)CF.1943-5509.0000521.

Tan, Y. and Wei, B. (2012). "Observed behaviors of a long and deep excavation constructed by cut-and-cover technique in Shanghai soft clay." *Journal of Geotechnical and Geoenvironmental Engineering*, Vol. 138, No. 1, pp. 69-88, DOI: 10.1061/(ASCE)GT.1943-5606.0000553.

Wang, Z.W., Ng, C. W. W., and Liu, G. B. (2005). "Characteristics of wall deflections and ground surface settlements in Shanghai." *Canadian Geotechnical Journal*, Vol. 42, No. 5, pp. 1243-1254, DOI: 10.1016/j.tust.2012.12.008.

Wu, S. H., Ching, J. Y., and Ou, C. Y. (2013). "Predicting wall displacements for excavations with cross walls in soft clay." *Journal of Geotechnical and Geoenvironmental Engineering*, Vol. 139, No. 6, pp. 914-927, DOI: 10.1061/(ASCE)GT.1943-5606.0000826.

Xu, Z. H. (2007). "Deformation behavior of deep excavations supported by permanent structures in Shanghai soft deposit." PhD Thesis, Shanghai Jiao Tong University, Shanghai, China (In Chinese).